Retraction

Retracted: Construction of the 3D Reconstruction System of Building Construction Scene Based on Deep Learning

Scientific Programming

This article has been retracted by Hindawi following an investigation undertaken by the publisher [1]. This investigation has uncovered evidence of one or more of the following indicators of systematic manipulation of the publication process:

(1) Discrepancies in scope

(2) Discrepancies in the description of the research reported

(3) Discrepancies between the availability of data and the research described

(4) Inappropriate citations

(5) Incoherent, meaningless and/or irrelevant content included in the article

(6) Peer-review manipulation

The presence of these indicators undermines our confidence in the integrity of the article's content and we cannot, therefore, vouch for its reliability. Please note that this notice is intended solely to alert readers that the content of this article is unreliable. We have not investigated whether authors were aware of or involved in the systematic manipulation of the publication process.

Wiley and Hindawi regrets that the usual quality checks did not identify these issues before publication and have since put additional measures in place to safeguard research integrity.

We wish to credit our own Research Integrity and Research Publishing teams and anonymous and named external researchers and research integrity experts for contributing to this investigation.

The corresponding author, as the representative of all authors, has been given the opportunity to register their agreement or disagreement to this retraction. We have kept a record of any response received.

References

[1] Z. Lu, "Construction of the 3D Reconstruction System of Building Construction Scene Based on Deep Learning," *Scientific Programming*, vol. 2021, Article ID 5839391, 9 pages, 2021.

Research Article

Construction of the 3D Reconstruction System of Building Construction Scene Based on Deep Learning

Zhou Lu [ID]

College of Architecture, South China University of Technology, Guangzhou 510641, Guangdong, China

Correspondence should be addressed to Zhou Lu; 201821005113@mail.scut.edu.cn

The increasing complexity and enormity of construction projects, as well as the fact that the actual operation of construction schedule management still mainly relies on traditional manual management methods, have led to low efficiency of construction schedule management and caused many construction projects to have cost overruns and legal disputes due to schedule delays. Existing 3D reconstruction algorithms often lead to significant voids, distortions, or blurred parts in the reconstructed 3D models, while the machine learning-based 3D reconstruction algorithms are often only to reconstruct simple separated objects and represent them as 3D boxes. A novel architecture of semisupervised 3D reconstruction algorithm is proposed. The algorithm iteratively improves the quality of the original 3D reconstruction model by training a generative adversarial network model to a converged state. Only the prior observed 2D images are required as weakly supervised samples, without any dependence on prior knowledge of the 3D structure shape or reference observations. Experimental results show that this algorithmic framework has significant advantages over the current state-of-the-art 3D reconstruction methods on the standard 3D reconstruction test set.

1. Introduction

A lot of research has been conducted on the topic of automated building construction schedule management with various technologies, but the existing research is hardly applicable to the complex building construction management practices [1–3]. These existing researches mainly focus on three aspects: management based on BIM (Building Information Modeling) technology [4–6], management based on RFID technology combined with BIM [7–9], and management based on Scan to BIM technology combined with 3D reconstruction technology [10–12]. For example, in schedule management, [13] conducted a study on building construction progress based on UAVs carrying Li DAR technology combined with BIM technology to achieve automatic monitoring of outdoor progress at building construction sites [14]. However, the existing automated construction schedule management approach suffers from two drawbacks.

For one, the high equipment dependence causes high management costs, such as Li DAR equipment generally costing tens of thousands of dollars, and the high cost of the UAV equipment required for tilt photography and the high maintenance costs during use make it difficult to apply in the actual management process [15–17].

Second, the poor operability of automation leads to a low level of automation, such as the use of Li DAR equipment has high requirements for the field environment [18], while the tilt photography method requires trained UAV professionals to operate and requires the implementation of work in specific airways and in practice to consider complex issues such as obstacle avoidance [19–22], requiring a high degree of human involvement.

Artificial intelligence technologies such as deep learning have gradually demonstrated strong productivity in the field of construction engineering in recent years [23–25], while a low-cost, automated, and intelligent construction schedule management method that can be applied to the construction site environment in combination with artificial intelligence technologies has yet to be studied [26]. In the field of computer vision and computer graphics, 3D reconstruction is a technique for recovering the shape, structure, and

appearance of real objects. Due to its rich and intuitive expressiveness, in this paper, we propose a 3D reconstruction algorithm based on semisupervised generative adversarial networks, which combine the advantages of traditional 3D reconstruction techniques with the latest machine learning principles of generative adversarial networks. By fine-tuning the adversarial training process of the 3D generative model and the 3D discriminative model simultaneously, the framework proposed in this paper can steadily refine the reconstruction quality of the reconstructed 3D objects in a semisupervised learning manner. On the basis of this algorithm, a 3D reconstruction cloud studio is also built to provide a convenient and accessible 3D reconstruction cloud service system to a wide range of users.

2. Related Work

The targets of 3D reconstruction can be some detached objects [27] or large scale scenes [28, 29]. For different reconstruction targets, researchers will try to present the reconstructed 3D models in different ways. Common forms of presentation include stereo body elements [6], point clouds [8], and a combination of mesh skeleton and surface textures [30]. In recent years, researchers have made great progress in the research of new methods for 3D reconstruction techniques.

This class of algorithms first performs feature matching based on two images, then uses the obtained dual-view reconstruction results to initialize the 3D model, adds new matching images and iterates repeatedly to perform triangular feature matching, and uses the beam leveling method to recover the motion structure. The time complexity of this class of algorithms is $O(n4)$, where n represents the number of observed cameras. The most representative algorithm in this class is VisualSFM [31], which further improves the computational performance and optimizes a large number of time-consuming steps including the beam leveling method.

However, such algorithms also have obvious limitations; they are all based on the important assumption that feature information is perfectly watchable across multiple viewpoints. If the spatial distance between the views is large, feature matching becomes extremely difficult due to local appearance changes or mutual occlusion. Another limitation is that if the surface of the object to be reconstructed lacks texture information, or if there are specular reflections on the surface, the feature matching process is likely to fail completely.

The most famous algorithm of this class is Kinect Fusion [32], which is able to continuously track and solve the pose information of the depth camera in 6 degrees of freedom by means of the detected depth information. The tracking accuracy of this method is significantly better than the 3D reconstruction method based on motion structure recovery (since this approach can only track the camera poses by matching features from frame to frame of color pictures). By iteratively fusing the depth and pose information into a dense global stereo model, the final output of the constructed 3D model is achieved. In Whelan's work [8], he further improves the tracking accuracy, tenacious robustness, and reconstruction quality based on KinectFusion. The improved algorithm uses techniques such as dense image frames corresponding to camera tracking of the model, sliding window point element fusion, and nonrigid surface deformation to obtain a higher quality 3D reconstructed model.

The limitations of this type of algorithm mainly lie in the existence of self-obscuration, light reflection, and depth sensor fusion errors, which can lead to significant voids, distortions, or blurred parts of the reconstructed 3D model.

The representative algorithm of this class is the 3D Recurrent Reconstruction Neural Network (3D-R2N2) [33] algorithm, which uses a deep CNN to learn the mapping relationship between the observed 2D image and the corresponding 3D shape of the target object from a large training dataset.

The most representative algorithm in this class is the 3D-GAN [7] algorithm. 3D-GAN algorithm introduces generative adversarial loss and uses it as a judging criterion to distinguish whether an object is real or reconstructed. Because 3D objects are highly structured, the use of generative adversarial loss is more effective than the traditional voxel-level independent heuristic judging criterion, which can capture the subtle differences of the 3D structure of the target object more accurately.

3. 3D Reconstruction Algorithm Is Based on Semisupervised Generative Adversarial Network

3.1. Algorithm Principle. Imagine an example where an observer wants to distinguish a real scene from an artificially reconstructed model of the scene. First, he would observe in the real 3D scene, and then he would also observe in the reconstructed 3D scene model, and the position and perspective of each observation would be the same as when he was in the real scene. If he observes a series of two-dimensional pictures in the reconstructed 3D scene model, which are exactly the same as what he observes in the real 3D scene, then it is actually extremely difficult for the observer himself to distinguish which is the real 3D scene and which is the reconstructed 3D scene model. In order to construct a 3D reconstruction algorithm, the differences between each set of 2D pictures were observed in the real scene, and the 2D pictures observed in the reconstructed scene model can be accumulated. If such differences are small enough for each observation position and viewpoint, this reconstructed 3D model can be considered to be of high quality. And from a quantitative point of view, the smaller the accumulated differences, the higher the quality of the reconstructed 3D model. This can be taken as the final criterion for judging the 3D reconstructed model. A more intuitive representation of this concept is shown in Figure 1.

From Figure 1, it can be seen that the improved algorithm runs significantly more efficiently than the original Apriori algorithm [34], especially when the support elucidation value is low.
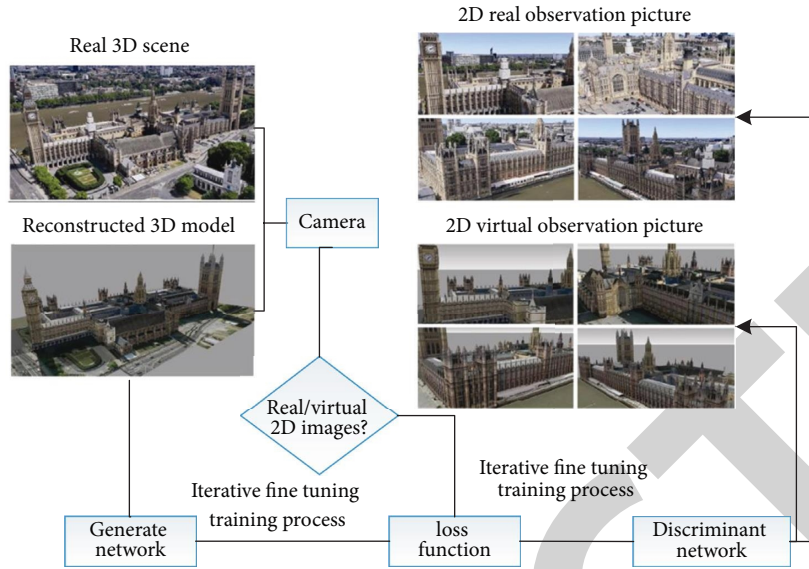
FIGURE 1: Principle and algorithm flow of 3D reconstruction algorithm based on GAN.

The discriminant network also estimates how likely it is that a particular sample is a sample synthesized by the generative network. When the entire generative adversarial network model reaches Nash equilibrium, i.e., the generative network can produce new samples with characteristics and distributions identical to those of the real samples, and the discriminant network outputs a discriminant probability of 0.5 for each pair of real and generative sample sets, the entire generative adversarial network model completes training and reaches convergence.

Combining the goal of 3D reconstruction with a generative adversarial network model, a new 3D reconstruction architecture is developed in this paper: a 3D reconstruction network based on semisupervised generative adversarial network (SS-GAN-3D). SS-GAN-3D is composed of a 3D model generation network and a 3D model discriminator network together. Here, the discriminator network can be imagined as the observer mentioned in the above example. In this way, the goal of the generative network is to reconstruct a 3D model that is extremely similar to the real 3D scene and try to confuse the discriminator network with this 3D scene model [35]. The goal of the discriminative network is to clearly distinguish the difference between the real 3D scene and the reconstructed 3D model. In this way, it also meets the measure of 3D reconstructed model quality given above. In conclusion, the new proposed architecture in this paper equivalently transforms the traditional 3D reconstruction solution problem into a machine learning problem that trains SS-GAN-3D and achieves convergence.

3.2. Algorithm Flow. When SS-GAN-3D is trained, an extremely rough 3D model is first generated as an initialization of the 3D model generation network. Here, the rough 3D model is represented in ".ply" format. The vertex, edge, and color information are stored in a triplet format [13]. The spatial stereo matching method estimates the depth

information of each point on the image of space by comparing the differences between adjacent observed image frames. Also, two-dimensional observation images truncated from the video stream are used to from the truth-value image dataset.

Since SS-GAN-3D requires 2D observation images from the reconstructed 3D model, the reconstructed 3D model is imported into the professional open-source 3D engine software blender and OpenDR [14]. OpenDR is a differentiable renderer that realistically approximates the realistic rendering from the 3D model to the 2D image and, at the same time, can provide the gradient change from the 2D image to the 3D model required by the backpropagation algorithm. It is a differentiable renderer that gives a realistic approximation of the rendering of the 3D model to the 2D image, while providing the gradient change from the 2D image to the 3D model required by the backpropagation algorithm. The differentiability of the renderer is essential, because the structure of the generative adversarial network needs the entire network to be fully differentiable, so that the gradient changes of the discriminative network can be passed back to update the generative network and form a complete circular iterative structure.

In Blender, a virtual camera can be set up with the exact same optical parameters as the real camera used to capture the video stream in the real 3D scene. When processing the real video stream, the camera's trajectory is already calculated. So, in Blender, the virtual camera is made to move along this trajectory and, using the OpenDR renderer, is observed at the same position and perspective as in the real scene and rendered to generate a 2D image. In this way, the same number of 2D virtual and real observation images can be obtained from the reconstructed 3D model and the real 3D scene, respectively.

With a collection of 2D virtual and real observation images, a discriminant network is used to distinguish whether they come from observations of the real 3D scene or

of the reconstructed 3D model. The loss value of the whole network is also calculated based on the loss function. With the network loss values, SS-GAN-3D can continue to fine-tune the training process to generate new 3D generative and 3D discriminative networks. The newly trained 3D generative network will reconstruct a new 3D model for the virtual camera to make observations. The virtual observation images from the new observations are fed together with the real original observation that the SS-GAN-3D is trained iteratively and continues to generate new 3D generative and discriminative networks until the overall loss value converges to a desired threshold.

3.3. Definition of Loss Function. The overall loss function of SS-GAN-3D contains two parts: the reconstruction loss ReconsL and the cross-entropy loss SS-GAN-3DL. So, the loss function can be written as

$$L_{\text{Overall}} = L_{\text{Recons}} + \lambda L_{\text{SS-GAN-3D}}, \tag{1}$$

where λ is the parameter value that regulates the reconstruction loss and cross-entropy loss weights.

In this paper, three quantitative measures of image quality [15] are selected for calculating the differences. Peak signal-to-noise ratio (PSNR) quantifies the picture different from the perspective of gray value fidelity. Structural similarity (SSIM) [16] quantitatively measures picture differences from the perspective of structural-level fidelity, while this metric refers to and simulates the judgment criteria of the human eye system for structural patterns. Normalized correlation (NC) [36], on the other hand, indicates the matrix similarity of pictures with the same dimension. Expressions of these 3 evaluation quantitative metrics are shown as follows:

$$\text{PSNR}(\mathbf{x}, \mathbf{y}) = 10 \lg \left(\frac{(\text{MAX}_I)^2}{\text{MSE}(\mathbf{x}, \mathbf{y})} \right), \tag{2}$$

where MAX_I represents the maximum value that can be obtained for each pixel in images x and y. $\text{MSE}(\mathbf{x}, \mathbf{y})$ represents the mean square error of picture x and y.

$$\text{SSIM}(\mathbf{x}, \mathbf{y}) = \frac{(2\mu_x\mu_y + C_1)(2\sigma_{xy} + C_2)}{(\mu_x^2 + \mu_y^2 + C_1)(\sigma_x^2 + \sigma_y^2 + C_2)}. \tag{3}$$

Among them, $\mu_x = 1/N \sum_{i=1}^{N} x_i$ and $\mu_y = 1/N \sum_{i=1}^{N} y_i$ represent the average gray values of pictures X and y. σ_x and σ_y represent the variance of pictures X and y. σ_{xy} represents the covariance of pictures X and y. Parameters C_1 and C_2 are two constants. When $\mu_x^2 + \mu_y^2$ or $\mu_x^2 + \mu_y^2$ is very close to 0, C_1 and C_2 can prevent divergent results from the final SSIM.

$$\text{NC}(\mathbf{x}, \mathbf{y}) = \frac{(\mathbf{x} \cdot \mathbf{y})}{\|\mathbf{x}\| \|\mathbf{y}\|}, \tag{4}$$

where $\mathbf{x} \cdot \mathbf{y}$ represents the inner product of matrices X and y, and operator$|.|$ represents the Euclidean norm of the vector.

Obviously, the structural similarity index of the two pictures is 0~1, and the normalized correlation index is −1~1. If SSIM index or NC index is very close to 1, the gap between X and Y is very small. For the peak signal-to-noise ratio index, the value of common pictures is 20~70 dB, which needs to be normalized by generalized sigmoid function.

$$E\_\text{Sig}(\text{PSNR}(\mathbf{x}, \mathbf{y})) = \frac{1}{1 + e^{-0.1(\text{PSNR}(x,y)-45)}}. \tag{5}$$

Therefore, the final reconstruction loss can be written in the following form:

$$L_{\text{Recons}} = \sum_{j=1}^{N} \left\{ \alpha \cdot \left[1 - E\_\text{Sig}\left(\text{PSNR}_{G_j F_j} \right) \right] + \beta \left(1 - \text{SSIM}_{G_j F_j} \right) + \gamma \cdot \left(1 - \text{NC}_{G_j F_j} \right) \right\}. \tag{6}$$

Among them, α, β, γ are parameters to adjust the proportion of PSNR, SSIM, and NC indicators in the overall loss value. Subscript $G_j F$ represents a pair of real and virtual observation two-dimensional pictures. The superscript n indicates the total number of such picture pairs in the picture set. Section 3.4 will discuss the cross-entropy loss of ss-gan-3d in detail in combination with the network structure.

3.4. Network Structure of SS-GAN-3D. For SS-GAN-3D, the discriminant network needs strong classification performance to deal with the complex two-dimensional slices generated by three-dimensional spatial projection. Therefore, this paper adopts ResNet-101 network [37] as the main structure of discrimination network. Typical ResNet networks adopt back normalization, which makes the whole training process more stable. However, the introduction of batch normalization operation makes the discriminant

network judge the mapping relationship between a batch of input and a batch of outputs. In ss-gan-3d, it is hoped to ensure the mapping relationship between single input and single output in the training process. In order to improve the training effect, the ReLu layer is also replaced with a parametritis ReLu layer. In order to improve the convergence performance, Adam solver is actually used to replace the random gradient descent (SGD) solver. In practical application, Adam solver can make ss-gan-3d train at a large learning rate. The detailed network hierarchy is shown in Figure 2.

According to the researchers' experiments, as of now, only the Wasserstein GAN (WGAN) [18] structures with the addition of gradient penalty restriction can successfully train complex generative and discriminative networks similar to the ResNet structure. Therefore, in this paper, we borrow the improved training algorithm of WGAN and apply it to the training process of SS-GAN-3D. The objective functions for
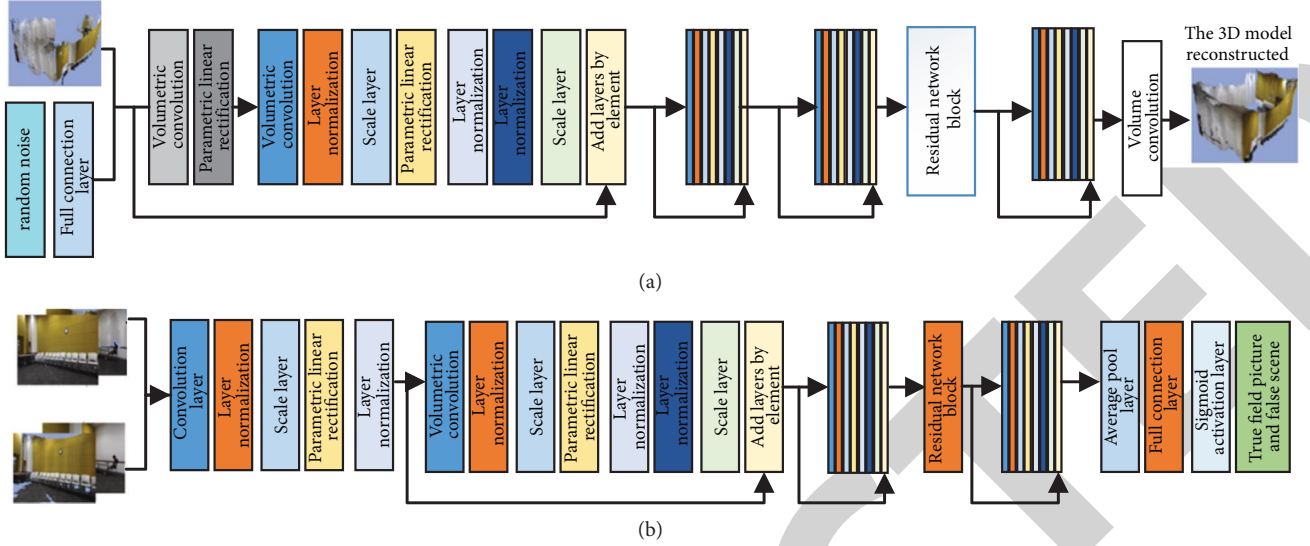
Figure 2: Structure of 3D generative and discriminative network. (a) 3D generation network structure. (b) Three-dimensional discriminant network structure.

training the generative network G and the discriminative network D are as follows:

$$\min_{G} \max_{D} \mathbb{E}_{x \sim \mathbb{P}_f} [D(x)] - \mathbb{E}_{i \sim \sim_g} [D(\tilde{x})], \tag{7}$$

where $\mathbb{P}_r$ represents the distribution of the real images, and $\mathbb{P}_g$ represents the distribution of the generated images. $\tilde{x}$ is the implicit output result of the generative network G. During the training of the original version of WGAN, the clipping of the weight values could easily lead to optimization failure, including network performance degradation, gradient explosion, or gradient disappearance. In the improved version of the gradient penalty, it is used as a looser constraint instead of simple weight cropping. So, the final cross-entropy loss of SS-GAN-3D is

$$L_{\text{SS-GAN-3D}} = \mathbb{E}_{x \sim \mathbb{P}_r} [D(x)] - \mathbb{E}_{\tilde{x} \sim \mathbb{P}_8} [D(\tilde{x})] \\ - \theta \mathbb{E}_{\hat{x} \sim \mathbb{P}_i} \left[\left(\left\| \nabla_{\hat{x}} D(\tilde{x}) \right\|_2 - 1 \right)^2 \right], \tag{8}$$

where θ is the parameter that regulates the percentage of the gradient penalty in the cross-entropy loss. $\mathbb{P}_{\tilde{x}}$ indicates that the value of the cross-entropy loss of the dataset formed by uniform sampling on the straight line between pairs of sample points obtained from the $\mathbb{P}_r$ and $\mathbb{P}_g$ distribution can quantitatively reflect the training process of SS-GAN-3D. The smaller this value, the smaller the Wasserstein distance between the real and virtual 2D observed images.

4. Simulation Results

4.1. Modeling Effect. Based on the system's high-speed camera's acquisition of image data from all angles of the real-time scenes of the construction site (as shown in Figure 3), the DLR-P system automatically analyzes the real-time

scenes of the project construction site and obtains the actual progress in the form of point cloud models for each of the three construction processes as shown in Figure 4. By cross-referencing the point cloud model with the idea BIM point cloud, the difference between the actual construction progress and the expected ideal progress is automatically calculated [33].

The read position in the leftmost figure indicates the comparison of the progress of sensor acquisition angle. By comparing the ideal BIM model converted into point cloud format (containing 3D information, construction schedule, and cost plan information) with the actual 3D point cloud model of the project site automatically identified by the 3D reconstruction technology based on deep learning, the difference of the construction site schedule relative to each plan is derived (as shown in Table 1). On this basis, the DLR-P system automatically adjusts the construction site plan to meet the total construction schedule and automatically provides on-site labor, material, and machinery resource responses according to the project volume and duration.

Operation speed: in order to realize the real-time automated management of the DLR-P system for construction projects, the time consumed by the 3D reconstruction process of various scenes was recorded, as shown in Table 2. The running speed is the time required from the moment when the high-speed camera acquires the image until the moment when the system outputs the final point cloud model. However, since the 3D reconstruction process mainly involves two parts, sparse reconstruction and dense reconstruction, the respective time consumed is related to many factors such as the number of reconstructed relevant images, image resolution, system background computing power, and the complexity of the images. Therefore, system operation speed recorded in the case study only represents the average speed required for the 3D reconstruction of the relevant scenes.

FIGURE 3: Real-time image data of the construction site from various angles: (a) construction of scaffolding on an exterior wall; (b) construction of protective net on an exterior wall; (c) construction of paint on the exterior wall.
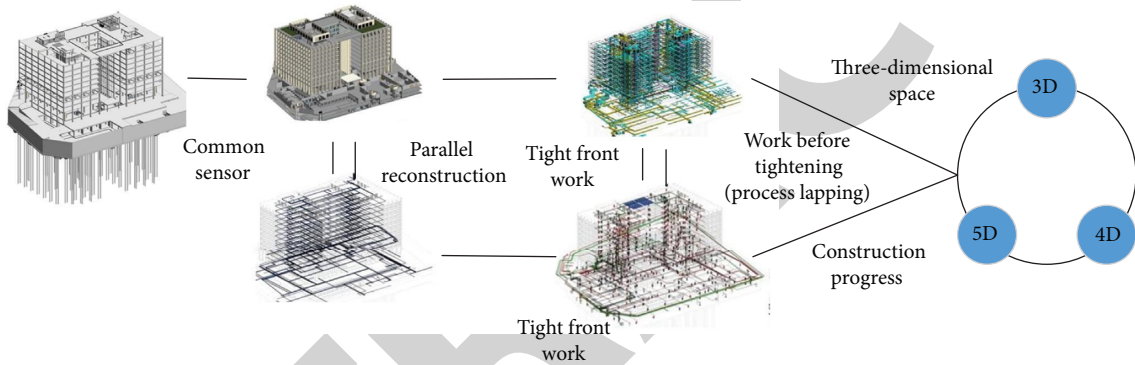

FIGURE 4: DLR-P system operation results.

TABLE 1: Progress plan variance and response.

Construction procedure		Construction of external wall scaffold	Construction of external wall protective net	Exterior wall coating construction
Schedule		4th floor	3th floor	4th floor
Actual progress		4th floor	4th floor	3th floor
Schedule variance		0	+1	−1
Plan adjustment		0	−1	+1
Resource response	Artificial	0	Workers—2	+3
	Material science	0	0	Paint +10 barrels
	Mechanics	0	0	0

4.2. System Operation. Operating costs: as shown in Table 2, the DLR-P system achieves fully automated construction schedule control without manual labor, and its main operating cost consists of the hardware cost of both the system backend and the system sensors, and its hardware equipment cost is only $33,000. The hardware cost is only $33,000, while the hardware cost of the management method based on the UAV method is about $370,000, and the cost of the handheld Li DAR equipment-based method is higher, about $820,000. During the case study of this project, only part of the construction of the project was studied, so if the whole project is controlled, the deployment cost of the DLR-P system should be higher than the above data, mainly due to the increase in the number of camera sensors. However, the DLR-P system proposed in this paper still has significant cost advantages compared to the other two schedule management implementations.

As depicted in Figure 5, the accuracy of calculation of construction volume is low, and the phenomena such as underinvestment or waste can occur. Based on 3D design and collaborative design technology, a more feasible and accurate construction plan can be simulated by the construction profession from the process design, thus providing the estimation profession with a relatively accurate base

TABLE 2: The speed of 3D reconstruction of our system.

| Construction procedure	Enter the number of images	Image fraction	Average operating speed (S)
Construction of external wall scaffold	10	1600×1200	31
		2400×1800	38
		3200×2400	55
	20	1600×1200	45
		2400×1800	68
		3200×2400	75
	30	1600×1200	69
		2400×1800	105
		3200×2400	152
Construction of external wall protective net	10	1600×1200	31
		2400×1800	43
		3200×2400	25
	20	1600×1200	40
		2400×1800	54
		3200×2400	59
	30	1600×1200	62
		2400×1800	92
		3200×2400	101
Rice square fish	10	1600×1200	23
		2400×1800	35
		3200×2400	40
	20	1600×1200	44
		2400×1800	59
		3200×2400	58
	30	1600×1200	53
		2400×1800	88
		3200×2400	105
Average value			61
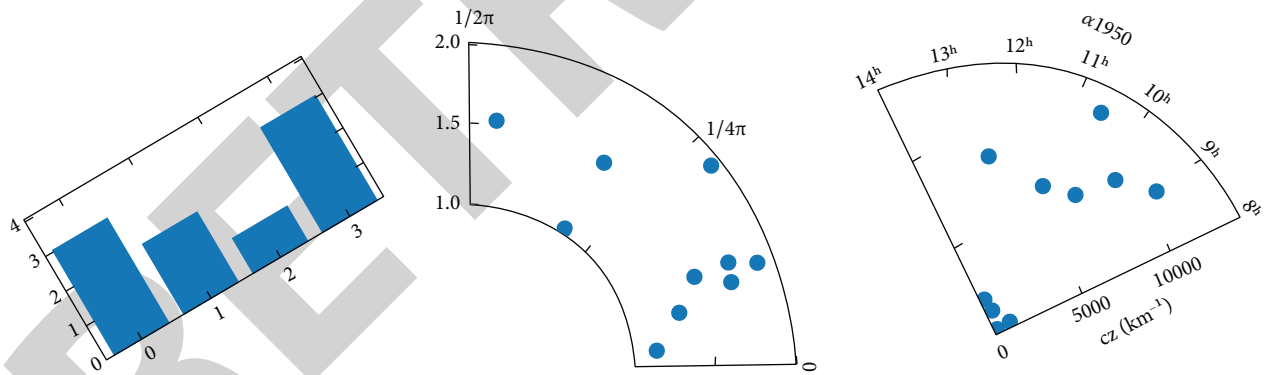
FIGURE 5: Different pattern generations.

information for the preparation of the estimated unit price and making the basis for the calculation of the whole project investment relatively accurate and reliable. In addition, the shared collaborative design platform can make use of the linkage of its various specialties to update the information on the changes in construction volume generated by design modifications at any time and link it with its own estimates. It can not only greatly improve the work efficiency, but also effectively reduce the unnecessary design errors due to the coordination of various professions [4]. By integrating more nongeometric information such as price parameters, market information, and price change factors into the 3D model, the construction process or project plan can be compared from

the perspective of engineering cost, effectively reducing design changes and making engineering investment more accurate and reasonable.

By integrating more nongeometric information such as price parameters, market information, and price change factors into the 3D model, the construction process or project plan can be compared from the perspective of engineering cost, effectively reducing design changes and making the project investment more accurate and reasonable. The construction camp layout is shown in Figure 6, which utilizes Infraworks' intuitive and concise 3D dynamic display function through terrain analysis.
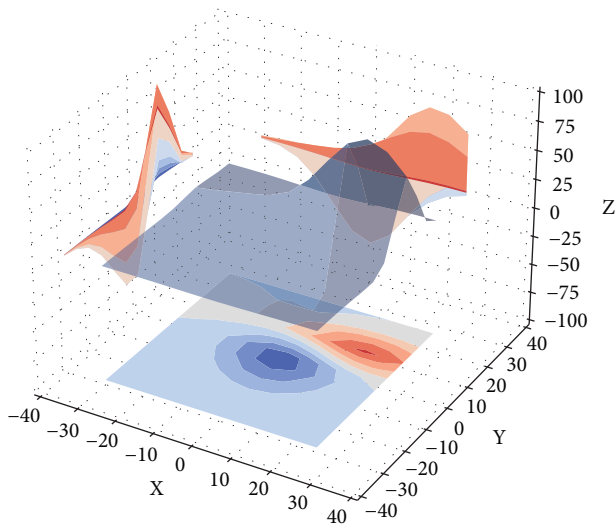
Figure 6: Different site terrain generations.

5. Conclusions

Existing 3D reconstruction algorithms often lead to the existence of obvious voids, distorted distortion, or blurred parts on the reconstructed 3D models, while the machine learning-based 3D reconstruction algorithms can often only reconstruct simple separated objects and represent them in the form of 3D boxes. So, all these algorithmic frameworks are far from sufficient for practical applications. Therefore, the focus of this paper is to use the production adversarial network principle to obtain high-quality 3D reconstruction results. Only the prior observed 2D images are required as weakly supervised samples, and there is no dependence on the prior knowledge of the 3D structure shape or the reference observation. Experimental results show that this algorithmic framework has significant advantages over the current state-of-the-art 3D reconstruction methods on the standard 3D reconstruction test set.

Data Availability

The datasets used in this paper are available upon request to the author.

Conflicts of Interest

The author declares no conflicts of interest regarding this work.

References

[1] L. Xin, X. Liu, Z. Yang, X. Zhang, Z. Gao, and Z. Liu, "Three-dimensional reconstruction of super-resolved white-light interferograms based on deep learning," *Optics and Lasers in Engineering*, vol. 145, no. 12, Article ID 106663, 2021.

[2] H. S. Cha and J. Kim, "A study on 3D/BIM-based on-site performance measurement system for building construction," *Journal of Asian Architecture and Building Engineering*, vol. 19, no. 6, pp. 574–585, 2020.

[3] X. D. Yang, B. H. Liu, and Y. Wang, "3D reconstruction of CT images based on isosurface construction," *Applied Mechanics and Materials*, vol. 10-12, pp. 503–507, 2008.

[4] M. R. Jahanshahi and S. F. Masri, "Adaptive vision-based crack detection using 3D scene reconstruction for condition assessment of structures," *Automation in Construction*, vol. 22, pp. 567–576, 2012.

[5] R. Li, T. Zeng, H. Peng, and S. Ji, "Deep learning segmentation of optical microscopy images improves 3-D neuron reconstruction," *IEEE Transactions on Medical Imaging*, vol. 36, no. 7, pp. 1533–1541, 2017.

[6] M. O. Malavé, C. A. Baron, S. P. Koundinyan et al., "Reconstruction of undersampled 3D non-Cartesian image-based navigators for coronary MRA using an unrolled deep learning model," *Magnetic Resonance in Medicine*, vol. 84, no. 2, pp. 800–812, 2020.

[7] J. Chen, Z. Kira, and Y. K. Cho, "Deep learning approach to point cloud scene understanding for automated scan to 3D reconstruction," *Journal of Computing in Civil Engineering*, vol. 33, no. 4, pp. 04019027.1–04019027.10, 2019.

[8] Y. Liu, S. Chen, and B. Guan, "Layout optimization of oil-gas gathering and transportation system in constrained three-dimensional space," *Chinese Science Bulletin*, vol. 65, no. 9, pp. 834–846, 2020.

[9] Y. Liu, S. Chen, B. Guan, and P. Xu, "Layout optimization of large-scale oil-gas gathering system based on combined optimization strategy," *Neurocomputing*, vol. 332, no. 7, pp. 159–183, 2019.

[10] B. Guan, S. Chen, Y. Liu, X. Wang, and J. Zhao, "Wave patterns of (2+1)-dimensional nonlinear Heisenberg ferromagnetic spin chains in the semiclassical limit," *Results in Physics*, vol. 16, Article ID 102834, 2019.

[11] X. Zhang, J. Yao, L. Dong, and N. Ye, "Research on 3D architectural scenes construction technology based on augmented reality," *Journal of Computational Methods in Science and Engineering*, vol. 21, no. 1, pp. 1–17, 2020.

[12] F. Chen, Mm Ad K. Muha, and S. H. Wang, "Three-dimensional reconstruction of CT image features based on multi-threaded deep learning calculation," *Pattern Recognition Letters*, vol. 136, pp. 309–315, 2020.

[13] D. Yu, S. Ji, J. Liu, and S. Wei, "Automatic 3D building reconstruction from multi-view aerial images with deep learning," *ISPRS Journal of Photogrammetry and Remote Sensing*, vol. 171, no. 2021, pp. 155–170, 2021.

[14] G. Fahim, K. Amin, and S. Zarif, "Single-view 3D reconstruction: a survey of deep learning methods," *Computers & Graphics*, vol. 94, no. 1, 2021.

[15] F. Kurz, S. Azimi, C. Y. Sheu, and P. D. Angelo, "Deep learning segmentation and 3D reconstruction of road markings using multiview aerial imagery," *International Journal of Geo-Information*, vol. 8, no. 1, 2019.

[16] G. Stuebl, C. Heindl, H. Bauer, and A. Pichler, "Deep learning based aesthetic evaluation of state-of-the-art 3D reconstruction techniques," in *Proceedings of the 3DBODY.TECH 2017 - 8th International Conference and Exhibition on 3D Body Scanning and Processing Technologies*, Montreal, Canada, Octobar, 2017.

[17] Q. Xie, X. Chen, L. Shen, and G. Li, "Brain microstructure reconstruction based on deep learning," *Systems Engineering-Theory & Practice*, vol. 38, no. 2, pp. 482–491, 2018.

[18] J. Teuwen, N. Moriakov, C. Fedon et al., "Deep learning reconstruction of digital breast tomosynthesis images for accurate breast density and patient-specific radiation dose estimation," *Medical Image Analysis*, vol. 71, no. 22, Article ID 102061, 2021.

[19] S. Sharma and V. Kumar, "Voxel-based 3D face reconstruction and its application to face recognition using

sequential deep learning," *Multimedia Tools and Applications*, vol. 79, no. 25, Article ID 17303, 2020.

[20] M. Pashaei, M. J. Starek, H. Kamangir, and J. Berryhill, "Deep learning-based single image super-resolution: an investigation for dense scene reconstruction with UAS photogrammetry," *Remote Sensing*, vol. 12, no. 11, p. 1757, 2020.

[21] T. Xie, C. Zhang, Z. Zhang, and K. Yang, "Utilizing active sensor nodes in smart environments for optimal communication coverage," *IEEE Access*, vol. 7, pp. 11338–13348, 2018.

[22] H. Li, D. Zeng, L. Chen, Q. Chen, M. Wang, and C. Zhang, "Immune Multipath Reliable Transmission with Fault Tolerance in Wireless Sensor Networks," in *Proceedings of the International Conference on Bio-Inspired Computing: Theories and Applications*, pp. 513–517, Springer, Singapore, Octobar, 2016.

[23] F. Alidoost, H. Arefi, and F. Tombari, "2D image-to-3D model: knowledge-based 3D building reconstruction (3DBR) using single aerial images and convolutional neural networks (CNNs)," *Remote Sensing*, vol. 11, no. 19, p. 2219, 2019.

[24] M. Liang and Z. Hu, "Reconstruction of 3D Building Models Based on Architectural Construction Drawings," in *Applied Mechanics and Materials*, vol. 336, pp. 1349–1355, Trans Tech Publications Ltd., Freienbach, Switzerland, 2013.

[25] Z. Zhang, C. Zhang, M. Li, and T. Xie, "Target positioning based on particle centroid drift in large-scale WSNs," *IEEE Access*, vol. 8, Article ID 127709, 2020.

[26] C. H. Cao, Y. N. Tang, D. Y. Huang, W. M. Gan, and C. Zhang, "IIBE: An Improved Identity-Based Encryption Algorithm for WSN Security," *Security and Communication Networks*, vol. 2021, Article ID 8527068, 8 pages, 2021.

[27] L. Wang, C. Zhang, Q. Chen et al., "A Communication Strategy of Proactive Nodes Based on Loop Theorem in Wireless Sensor Networks," in *Proceedings of the 2018 9th International Conference on Intelligent Control and Information Processing (ICICIP)*, pp. 160–167, IEEE, Wanzhou, China, November, 2018.

[28] F. Bosché, "Plane-based registration of construction laser scans with 3D/4D building models," *Advanced Engineering Informatics*, vol. 26, no. 1, pp. 90–102, 2012.

[29] H. Son, S. Lee, and C. Kim, "What drives the adoption of building information modeling in design organizations? An empirical investigation of the antecedents affecting architects' behavioral intentions," *Automation in construction*, vol. 49, no. 4, pp. 92–99, 2015.

[30] C. J. Chun-Jen Tsai and A. K. Katsaggelos, "Sequential construction of 3-D-based scene description," *IEEE Transactions on Circuits and Systems for Video Technology*, vol. 10, no. 4, pp. 576–584, 2000.

[31] C. Liu and G. Liu, "Characterization of pore structure parameters of foam concrete by 3D reconstruction and image analysis," *Construction and Building Materials*, vol. 267, Article ID 120958, 2020.

[32] C. Zhang, T. Xie, K. Yang et al., "Positioning optimisation based on particle quality prediction in wireless sensor networks," *IET Networks*, vol. 8, no. 2, pp. 107–113, 2019.

[33] W. Boy, R. Imani, M. Chari, W. Purba, and J. Melasari, "Risk assesment of housing reconstruction project community-based construction after the earthquake," *Journal of Physics: Conference Series*, vol. 1339, no. 1, Article ID 012001, 2019.

[34] I. I. Tanaka, S. F. d. R. Tonhom, E. d. F. Taipeiro et al., "Grupo interdisciplinar: construção de Unidade educacional sistematizada em aprendizagem baseada em problemas," *O Mundo da Saúde*, vol. 37, no. 1, pp. 78–83, 2013.

[35] D. Wu, C. Zhang, L. Ji, R. Ran, H. Wu, and Y. Xu, "Forest fire recognition based on feature extraction from multi-view images," *Traitement du Signal*, vol. 38, no. 3, pp. 775–783, 2021.

[36] S.-I. Lee, N.-H. Kwon, and Y.-S. Cho, "A case study of BIM-based framework on constructability tasks," *Journal of the Korea Institute of Building Construction*, vol. 10, no. 5, pp. 45–54, 2010.

[37] J. An, G. Cho, and I. Yeo, "A study on the improvement plan of classification system for beam and slab of fire resistance construction in building's law," *Journal of the Korean Society of Hazard Mitigation*, vol. 20, no. 1, pp. 203–210, 2020.